On the sound field of a shallow spherical shell in an infinite baffle

Tim Mellow[a)]
Nokia UK Ltd., Farnborough, Hants GU14 0NG, United Kingdom

Leo Kärkkäinen
Nokia Research Center, Helsinki, Finland

(Received 28 August 2006; revised 31 January 2007; accepted 16 February 2007)

A method is presented for calculating the far field sound radiation from a shallow spherical shell in an acoustic medium. The shell has a concentrated ring mass boundary condition at its perimeter representing a loudspeaker voice coil and is excited by a concentrated ring force exerted by the end of the voice coil. A Green's function is developed for a shallow spherical shell, which is based upon Reissner's solution to the shell wave equation [Q. Appl. Math. **13**, 279–290 (1955)]. The shell is then coupled to the surrounding acoustic medium using an eigenfunction expansion, with unknown coefficients, for its deflection. The resulting surface pressure distribution is solved using the King integral together with the free space Green's function in cylindrical coordinates. In order to eliminate the need for numerical integration, the radiation (coupling) integrals are solved analytically to yield fast converging expansions. Hence, a set of simultaneous equations is obtained which is solved for the coefficients of the eigenfunction expansion. These coefficients are finally used in formulas for the far field sound radiation. © *2007 Acoustical Society of America.* [DOI: 10.1121/1.2715464]

PACS number(s): 43.58.Ta, 43.20.Rz, 43.20.Tb, 43.40.Ey, 43.38.Ja [LLT] Pages: 3527–3541

I. INTRODUCTION

The shallow spherical shell is a somewhat commonly used structure in acoustical transducers and methods for calculating its eigenfrequencies in a vacuum have long been established,[1–5] but little analytical work appears to have been done for calculating the radiated sound pressure when surrounded by a fluid medium. This is perhaps slightly surprising considering the extensive usage of shells in audio transducers ranging from miniature loudspeakers in mobile devices to hi-fi midrange units and high power tweeters used in PA systems. Although the use of boundary or finite element modeling is now fairly widespread in the transducer industry, analytical solutions are particularly useful in providing benchmarks for such models so that the element size and meshing geometry can be optimized. This enables more complicated geometries to be modeled with confidence.

A more general aim of this paper, though, is to provide formulas which enable very fast calculations and show the relationships between the various parameters. For example, it is useful to know how great the effect of the acoustic loading actually is and whether acoustic resistance can be used to control the modes. However, neither the ring-surround nor any other structures in a typical loudspeaker, such as the magnet and basket, are included in the model: The shell is assumed to be open to free space on both sides of the baffle which extends to infinity from the rim, although a specific acoustic impedance is included which can be used to model distributed impedances such as external damping (e.g., a mesh) or mixed mass and resistance in the form of an array of sound outlet holes. (Internal damping can be modeled using complex flexural rigidity.[6]) This specific impedance can also be used in a slightly less rigorous manner to represent lumped parameters such as the compliance of a rear cavity.

Reissner[1] provides a method for calculating the *in vacuo* eigenfrequencies based on the assumption that, if the shell is shallow, the radial and tangential components of the displacement can be ignored. Furthermore, it is suggested that this is a reasonable assumption for height/radius ratios up to around 0.25. A similar assumption is made here for the acoustic radiation whereby the shell is treated as a flat circular radiator. From a study made by Suzuki,*et al.*,[7] it can be concluded that this is a reasonable assumption up to $ka=5$ for the same range of height/radius ratios. This is somewhat fortuitous because it allows a small amount of curvature to be applied in order to increase rigidity (or reduce mass) relative to a flat plate without deviating too far from the theoretically flat far-field on-axis response of a flat piston up to the first break-up mode. Furthermore, the thin shallow shell assumptions simplify the formulation.

Jones *et al.*[4] provide an alternative approach for calculating the eigenfrequencies, which allows axial asymmetry while Thomas *et al.*[5] investigate nonlinear vibrations. Suzuki *et al.*[8] calculate the sound radiated from a fluid-loaded plate using an elastic boundary condition at the perimeter to model the suspension. However, in the current analysis it is assumed that, above the suspension resonance, the coil mass dominates, so this is included as a boundary condition too, together with the electrical/mechanical damping resistance. The Green's function in cylindrical coordinates is used, instead of the more common spherical form $e^{ikr}/(4\pi r)$, in or-

[a)]Electronic mail: tim.mellow@nokia.com

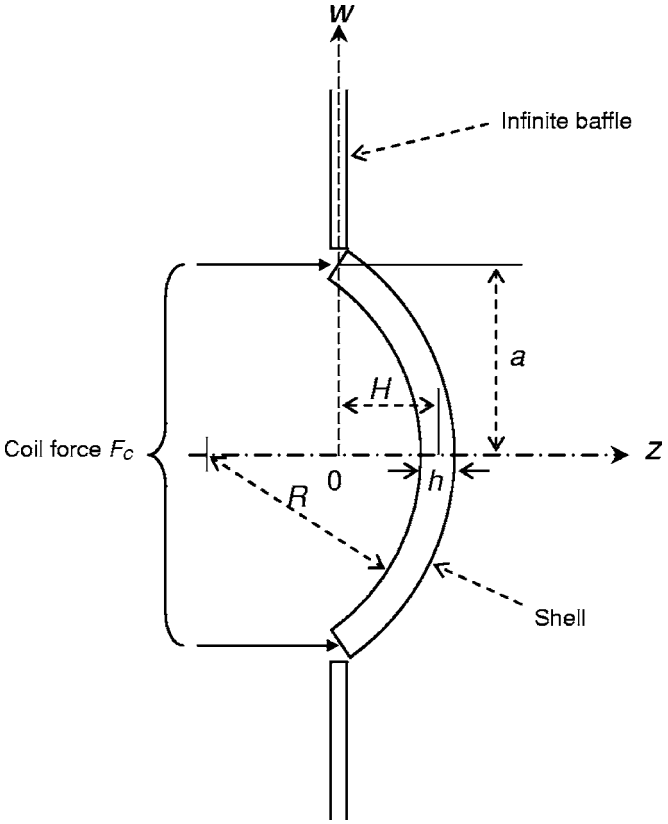

FIG. 1. Geometry of the shell.

der to facilitate the solution of the integrals and so avoid the need for numerical calculation of nested integrals.

A crucial factor in the solution of problems of sound radiation from monopole sources with arbitrary velocity distributions is the choice of trial function for the velocity or displacement at the source. In cases where the velocity is either zero or infinity at the perimeter,[9,10] a trial function based upon Bouwkamp's solution[11] to the free space wave equation in oblate spheroidal coordinates has been shown to be particularly useful, especially when calculating the near field pressure. The same applies to the trial function for the source pressure in dipole sources.[12] However, in this case, the velocity has a finite nonzero value at the shell perimeter so an eigenfunction (Bessel) expansion is used instead in order to avoid potential problems with convergence.

II. SOLUTION OF THE DYNAMIC *IN VACUO* SHELL WAVE EQUATIONS

A. Shell boundary conditions

The equations that follow are written in axisymmetric cylindrical coordinates, with w as the radial ordinate and z as the axial ordinate. An elastic spherical shell with radius a and thickness h, as shown in Fig. 1, is set in an infinite baffle of the same thickness with its center located on the z axis, which forms the axis of symmetry. Within its perimeter, the shell is homogeneous and continuous and is fabricated from an isotropic material with a Poisson's ratio of $\nu=0.3$.

For the purpose of this model, the shell and coil former are formed from the same piece of material and have the same thickness. Hence, at the rim, there is assumed to be neither bending nor radial strain. Also, the coil force $\tilde{F}_C$ is applied to the rim in the z direction. The tilde denotes a harmonically time varying quantity where the factor $e^{i\omega t}$ is suppressed. A separate suspension is assumed to be attached either to the coil or directly to the shell perimeter. It is assumed to provide pure linear stiffness K_S in the z direction with mechanical damping R_M and its mass is included with that of the voice coil, which is denoted by M_C. The coil driving force $\tilde{F}_C$ is used as the input in a wave equation for the shell, which is defined in terms of the input voltage $\tilde{e}_{\text{in}}$ by

$$\tilde{F}_C = Bl\tilde{e}_{\text{in}}/R_E, \tag{1}$$

where R_E is the electrical resistance of the coil and Bl is the magnetic flux coil length product. The total damping resistance R_S is then given by

$$R_S = R_M + (Bl)^2/R_E. \tag{2}$$

The deflection $\tilde{\eta}(w)$ of the shell is then be used as a parameter to couple it to the surrounding loss-free acoustic medium. Hence the shell and free space wave equations must be solved simultaneously.

B. Nonhomogeneous shell wave equation

Reissner's dynamic shell wave equations[1] are obtained by adding an axial inertia term to the static shell equations[13] while ignoring radial or tangential terms. Suppose that the spherical shell surface, as shown in Fig. 1, is defined by

$$z = R(\sqrt{1-w^2/R^2} - \sqrt{1-a^2/R^2}) \approx \frac{a^2-w^2}{2R}, \quad R > 2a \text{ (for surface average error} < 10\,\%). \tag{3}$$

The following simultaneous steady-state equations with an applied external harmonic load distribution $\tilde{p}(w)$ need to be solved for the displacement $\tilde{\eta}$ and an Airy stress function $\tilde{F}$,

$$D\nabla^4\tilde{\eta}(w) - \frac{1}{R}\nabla^2\tilde{F}(w) - \omega^2\rho_S h\tilde{\eta}(w) = \tilde{p}(w), \tag{4}$$

$$\nabla^4\tilde{F}(w) + \frac{hY}{R}\nabla^2\tilde{\eta}(w) = 0, \tag{5}$$

where, in the case of axisymmetric polar coordinates, the Laplace operator is given by

$$\nabla^2 = \frac{\partial^2}{\partial w^2} + \frac{1}{w}\frac{\partial}{\partial w} \tag{6}$$

and D is the flexural rigidity given by

$$D = \frac{Yh^3}{12(1-\nu^2)}, \tag{7}$$

where h is the thickness of the shell, Y is the Young's modulus of elasticity of the shell material, ν is its Poisson's ratio, and ρ_S is its density. The radius of curvature R is related to the dome height H by

$$R = \frac{a^2}{2H}. \tag{8}$$

Let a harmonic function $\tilde{\psi}$ be defined which satisfies

$$\nabla^2 \tilde{\psi} = 0 \tag{9}$$

so that

$$\nabla^2 \tilde{F}(w) = -\frac{hY}{R}(\tilde{\eta}(w) - \tilde{\psi}), \tag{10}$$

which, in turn, satisfies Eq. (5). Substituting Eq. (10) in Eq. (4) gives the following single steady-state homogeneous wave equation for the deflection:

$$\left(D\nabla^4 + \frac{hY}{R^2} - \omega^2 \rho_s h\right)\tilde{\eta}(w) = \frac{hY}{R}\tilde{\psi} + \tilde{p}(w). \tag{11}$$

C. Homogeneous shell wave equation

Suppressing the external pressure term in Eq. (11) yields the homogeneous wave equation, which can be written in the Helmholtz form as follows:

$$(\nabla^4 - k_S^4)\tilde{\eta}(w) = \frac{hY}{RD}\tilde{\psi}, \tag{12}$$

where k_S is the wave number of the shell which is given by

$$k_S = \frac{2\pi}{\lambda_S} = \frac{\omega}{c_S} = \left(\frac{\rho_S h}{D}\omega^2 - \frac{hY}{R^2 D}\right)^{1/4} \tag{13}$$

or, using Eqs. (7) and (8), it can be written

$$k_S^4 = \frac{\rho_S h}{D}\omega^2 - \frac{\xi^4}{a^4}, \tag{14}$$

where

$$\xi^4 = 48(1 - \nu^2)H^2/h^2. \tag{15}$$

The speed of sound c_S in the shell is given by

$$c_S = \omega/k_S. \tag{16}$$

As with a plate, high frequencies travel faster in the shell than low frequencies, which makes the shell a dispersive medium. It can be seen that at some transition frequency f_{INF} the speed of sound and hence also the wavelength become infinite. Below f_{INF}, the wavelength is complex with a 45° phase angle. Hence static solutions[13,14] are usually written in terms of Thomson (a.k.a. Kelvin) functions, which can be defined as Bessel functions with $e^{i\pi/4}$ in their arguments.[15] The transition frequency is given by

$$f_{\mathrm{INF}} = \frac{H}{\pi a^2}\sqrt{\frac{Y}{\rho_S}}. \tag{17}$$

Reissner[1] shows that the solutions to Eqs. (4) and (5) are eigenfunctions of the form

$$\tilde{\eta}_n(w) = \tilde{C}_{1n}J_0(k_S w) + \tilde{C}_{2n}Y_0(k_S w) + \tilde{C}_{3n}I_0(k_S w) + \tilde{C}_{4n}K_0(k_S w) + \tilde{C}_{5n}, \tag{18}$$

$$\tilde{F}_n(w) = -\frac{2HhY}{k_S^2 a^2}(\tilde{C}_{1n}J_0(k_S w) + \tilde{C}_{2n}Y_0(k_S w) - \tilde{C}_{3n}I_0(k_S w) - \tilde{C}_{4n}K_0(k_S w)) + \frac{\rho_S h a^2 \omega^2}{8H}\tilde{C}_{5n}w^2 + \tilde{C}_{6n}\log w + \tilde{C}_{7n}, \tag{19}$$

where $\tilde{C}_{5n} = \tilde{\psi}_n$ and n is the eigenindex. A useful alternative derivation to that of Reissner is provided by Gradowczyk,[14] which uses the auxiliary equation method to solve the simultaneous differential equations. In Eqs. (18) and (19), the arguments of the Bessel functions J, Y, I, and K can only have specific values, or eigenvalues, which satisfy the boundary conditions. The eigenvalues of the system are represented by setting $k_S a = \beta_n$. The eigenvalues and constants are then determined by applying boundary conditions, which are evaluated with help from the following identities:[15]

$$\frac{d}{dw}Z_0(k_S w) = \mp k_S Z_1(k_S w), \tag{20}$$

$$\frac{d^2}{dw^2}Z_0(k_S w) = k_S^2\left(\pm\frac{Z_1(k_S w)}{k_S w} \mp Z_0(k_S w)\right), \tag{21}$$

$$\frac{d^3}{dw^3}Z_0(k_S w) = k_S^3\left\{\left(1 \mp \frac{2}{k_S^2 w^2}\right)Z_1(k_S w) \pm \frac{Z_0(k_S w)}{k_S w}\right\}, \tag{22}$$

where Z can represent either J (upper sign) or I (lower sign).

D. Eigenvalues of the shell in a vacuum

1. Boundary condition of continuity at the center

In this configuration, $\tilde{\eta}_n$ and $\tilde{F}_n$ must be continuous at the apex ($w=0$). Therefore we have

$$\tilde{C}_{2n} = \tilde{C}_{4n} = \tilde{C}_{6n} = 0. \tag{23}$$

2. Boundary condition of zero bending at the perimeter

There is assumed to be zero bending at the perimeter. Therefore

$$\frac{\partial}{\partial w}\tilde{\eta}_n(w)\bigg|_{w=a} = -\frac{\beta_n}{a}\tilde{C}_{1n}J_1(\beta_n) + \frac{\beta_n}{a}\tilde{C}_{3n}I_1(\beta_n) = 0 \tag{24}$$

so that

$$\tilde{C}_{3n} = \frac{J_1(\beta_n)}{I_1(\beta_n)}\tilde{C}_{1n}. \tag{25}$$

3. Boundary condition of zero radial strain at the perimeter

At the perimeter, there is assumed to be zero radial strain.[13] Hence

$$\left(\frac{\partial^2}{\partial w^2}-\frac{\nu}{w}\frac{\partial}{\partial w}\right)\widetilde{F}_n(w)\Big|_{w=a}$$
$$=\frac{2hHY}{a^2}\left\{\widetilde{C}_{1n}\left(J_0(\beta_n)-\frac{1+\nu}{\beta_n}J_1(\beta_n)\right)+\widetilde{C}_{3n}\left(I_0(\beta_n)-\frac{1+\nu}{\beta_n}I_1(\beta_n)\right)\right\}+(1-\nu)\omega_n^2\frac{a^2\rho_S h}{4H}\widetilde{C}_{5n}=0, \quad (26)$$

where from Eq. (14)

$$\omega_n^2=\frac{D(\beta_n^4+\xi^4)}{a^4\rho_S h} \quad (27)$$

so that

$$\widetilde{C}_{5n}=-\frac{2\xi^4}{(1-\nu)(\beta_n^4+\xi^4)}\left\{\widetilde{C}_{1n}\left(J_0(\beta_n)-\frac{1+\nu}{\beta_n}J_1(\beta_n)\right)+\widetilde{C}_{3n}\left(I_0(\beta_n)-\frac{1+\nu}{\beta_n}I_1(\beta_n)\right)\right\}. \quad (28)$$

4. Coil impedance at the perimeter

The coil mass and suspension produce an axially symmetric (vertical) shear force[13] resultant Q_v at the perimeter. Hence, assuming that $a \ll R$,

$$\widetilde{Q}_{vn}(w)\big|_{w=a}=\left(\widetilde{Q}_n(w)+\widetilde{N}_n(w)\frac{w}{R}\right)_{w=a}=(\omega_n^2 M_C-K_S-i\omega_n R_S)\frac{\widetilde{\eta}_n(a)}{2\pi a}, \quad (29)$$

where M_C is the mass of the coil and its former, K_S is the stiffness of the suspension, and R_S is the total damping resistance. Also, the shear force is defined by[13]

$$\widetilde{Q}_n(w)=-D\frac{\partial}{\partial w}\nabla^2\widetilde{\eta}_n(w)\big|_{w=a}=-\frac{\beta_n^3}{a^3}D(\widetilde{C}_{1n}J_1(\beta_n)+\widetilde{C}_{3n}I_1(\beta_n)) \quad (30)$$

and the radial membrane force is defined by

$$\widetilde{N}_n(w)=-\frac{1}{w}\frac{\partial}{\partial w}F(w)=-\frac{2HhY}{a^2\beta_n}\left(\widetilde{C}_{1n}J_1(\beta_n)+\widetilde{C}_{3n}I_1(\beta_n)\right)-\widetilde{C}_{5n}\frac{\omega_n^2 a^2\rho_S h}{4H} \quad (30a)$$

so that

$$\widetilde{C}_{5n}=-\widetilde{C}_{1n}J_0(\beta_n)-\widetilde{C}_{3n}I_0(\beta_n)-(\beta_n^4+\xi^4)\times\frac{4\widetilde{C}_{1n}J_1(\beta_n)-\beta_n\left(\widetilde{C}_{1n}J_0(\beta_n)+\widetilde{C}_{3n}I_0(\beta_n)\right)}{\beta_n\left(\left(1+\frac{M_C}{M_S}\right)(\beta_n^4+\xi^4)-\frac{a^2K_S}{\pi D}-i\frac{R_S}{\pi}\sqrt{\frac{\beta_n^4+\xi^4}{\rho_S hD}}\right)}. \quad (31)$$

The surface area S of a shallow shell is

$$S=2\pi R(R-\sqrt{R^2-a^2})\approx\pi a^2, \quad R>2a. \quad (32)$$

The total mass M_S of the shell is therefore

$$M_S=\pi a^2\rho_S h. \quad (33)$$

Let ω_0 be a notional angular frequency, representing the suspension resonance of a perfectly rigid shell (including its coil mass). Hence, the stiffness may be defined by

$$K_S=(M_S+M_C)\omega_0^2. \quad (34)$$

From Eqs. (27), (33), and (34), the stiffness can be expressed as follows:

$$K_S=\frac{\pi D}{a^2}\left(1+\frac{M_C}{M_S}\right)(\beta_0^4+\xi^4), \quad (35)$$

where β_0 is a notional zeroth eigenvalue. Also, let the Q of this fundamental resonance be defined by

$$Q_S=\sqrt{(M_S+M_C)K_S}/R_S. \quad (36)$$

E. Calculation of the eigenvalues

Equating Eq. (28) with Eq. (31) and inserting the expressions for K_S and R_S from Eqs. (35) and (36), respectively, together with the identity for $\widetilde{C}_{3n}$ from Eq. (25) produces a characteristic equation that can be solved for the eigenvalues

$$\left(1+\frac{M_C}{M_S}\right)\left(\beta_n^4-\beta_0^4-i\frac{\sqrt{(\beta_0^4+\xi^4)(\beta_n^4+\xi^4)}}{Q_S}\right)\times\left\{((1-\nu)\beta_n^4-(1+\nu)\xi^4)W(\beta_n)+4\xi^4\frac{1+\nu}{\beta_n}J_1(\beta_n)I_1(\beta_n)\right\}-(1-\nu)(\beta_n^4+\xi^4)^2\left(W(\beta_n)-\frac{4}{\beta_n}J_1(\beta_n)I_1(\beta_n)\right)=0, \quad (37)$$

where

$$W(\beta_n)=J_0(\beta_n)I_1(\beta_n)+J_1(\beta_n)I_0(\beta_n).$$

and the notional zeroth eigenvalue β_0 is defined by

$$\beta_0^4=\frac{a^2M_S}{\pi D}\omega_0^2-\xi^4, \quad (38)$$

which is then used as a parameter in the characteristic equation (not a solution) to define the suspension stiffness.

F. Eigenvalues with zero load at the perimeter

If there is no loading at the perimeter, then $M_C=0$ and $\omega_0=0$. Eq. (37) reduces to

$$(\beta_n^4+\xi^4)\left\{W(\beta_n)-2\frac{(1-\nu)\beta_n^4+2\xi^4}{\beta_n\xi^4}J_1(\beta_n)I_1(\beta_n)\right\}. \quad (39a)$$

For zero height, setting $\xi^4=0$, yields the following eigenvalues

$$\beta_1 = 0 \quad \beta_2 = 3.8317 \quad \beta_3 = 7.0156$$

$$\beta_4 = 10.174 \quad \beta_5 = 13.324.$$

whereas setting $\xi^4 = \infty$ gives

$$\beta_1 = e^{i\pi/4}\infty \quad \beta_2 = 5.9057 \quad \beta_3 = 9.1969$$

$$\beta_4 = 12.402 \quad \beta_5 = 15.580.$$

Using the following asymptotic expressions[16] for the Bessel functions in Eq. (37),

$$J_\nu(z)\Big|_{z\to\infty} \approx \sqrt{\frac{2}{\pi z}}\cos\left(z - \frac{(2\nu+1)}{4}\pi\right), \tag{39b}$$

$$I_\nu(z)\Big|_{z\to\infty} \approx \sqrt{\frac{1}{2\pi z}}e^z, \tag{40}$$

it can be shown that

$$\beta_n|_{n\to\infty} \approx (n - 3/4)\pi, \quad H/h = 0.$$
$$\beta_n|_{n\to\infty} \approx n\pi, \quad H/h = \infty. \tag{41}$$

From Eq. (14), the eigenfrequencies are obtained as follows:

$$f_n = \frac{h}{4\pi a^2}\sqrt{\frac{Y}{3\rho_S}\left(\frac{\beta_n^4}{(1-\nu^2)} + 48\frac{H^2}{h^2}\right)}. \tag{42}$$

Not surprisingly, when $H=0$, Eq. (42) reduces to the eigenfrequency equation for a plate. However, when $H > 10h$, say, the equation for the fundamental shell eigenfrequency in asymptotic form becomes

$$f_2 \approx \frac{H}{\pi a^2}\sqrt{\frac{Y}{\rho_S}}, \quad H > 10h$$
$$= \frac{1}{2\pi R}\sqrt{\frac{Y}{\rho_S}} = f_{\mathrm{INF}}. \tag{43}$$

This slightly surprising result, due to Reissner,[1] indicates that when the height of the apex is much greater than the wall thickness, the fundamental resonant frequency (second eigenfrequency f_2) of the shell is dependent only upon its radius of curvature and material properties regardless of the wall thickness. (This does not apply to the first eigenfrequency, or piston eigenfrequency, which remains zero.) This effect is demonstrated in Fig. 2 where the eigenfrequencies are plotted against the height to thickness ratio. The eigenfrequencies f_n are normalized to the fundamental eigenfrequency f_{P2} of the corresponding flat circular plate where

$$f_{P2} = \frac{\beta_2^2 h}{4\pi a^2}\sqrt{\frac{Y}{3(1-\nu^2)\rho_S}}, \quad \beta_2 = 3.8317. \tag{44}$$

On the left-hand side of the plot, the eigenfrequencies converge to those of the flat circular plate with the same boundary conditions. On the right-hand side, the asymptotic value is $f_{\mathrm{INF}}/f_{P2} = 0.4502H/h$. However, $f_1 = 0$ for any height because the shell is free to float through space and so this is the "piston" eigenfrequency.

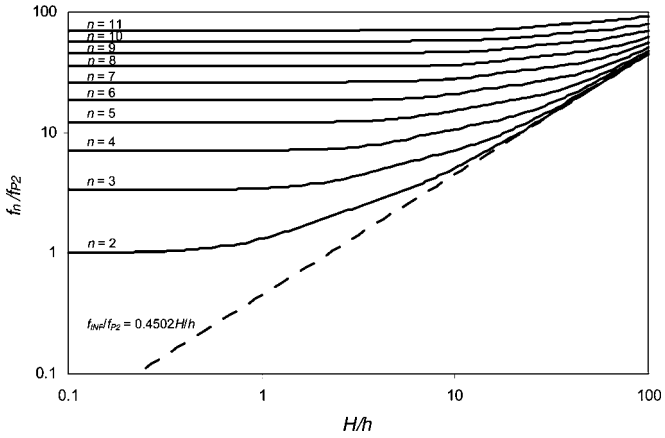

FIG. 2. Eigenfrequencies of a shallow spherical shell with zero load at the perimeter.

G. Eigenvalues with infinite load at the perimeter

If $M_C = \infty$ and $\omega_0 = 0$, then the shell's dynamic axial movement is blocked, although it can still move through space at constant velocity and hence returns a zero value for the 1st eigenfrequency, Eq. (38) reduces to:

$$(\beta_n^4 + \xi^4)\left\{W(\beta_n) + \frac{4(1+\nu)\xi^4 J_1(\beta_n)I_1(\beta_n)}{\beta_n((1-\nu)\beta_n^4 - (1+\nu)\xi^4)}\right\} = 0 \tag{45}$$

which is identical to Reissner's equation for a clamped shell, except for the factor $(\beta_n^4 + \xi^4)$ which gives the piston mode. For zero height, setting $\xi^4 = 0$, yields the following eigenvalues

$$\beta_1 = 0 \quad \beta_2 = 3.1962 \quad \beta_3 = 6.3064 \quad \beta_4 = 9.4395$$

$$\beta_5 = 12.577$$

whereas setting $\xi^4 = \infty$ gives

$$\beta_1 = e^{i\pi/4}\infty \quad \beta_2 = 5.9057 \quad \beta_3 = 9.1969$$

$$\beta_4 = 12.402 \quad \beta_5 = 15.580$$

Again, using the identities of Eqs. (39) and (40), expressions for the large eigenvalues can be obtained:

$$\beta_n|_{n\to\infty} \approx (n-1)\ \pi, \quad H/h = 0$$
$$\beta_n|_{n\to\infty} \approx n\pi, \quad H/h = \infty \tag{46}$$

In Fig. 3, the eigenfrequencies f_n of a simply supported shell are normalized to the fundamental eigenfrequency f_{P2} of the corresponding flat circular plate where

$$f_{P2} = \frac{\beta_2^2 h}{4\pi a^2}\sqrt{\frac{Y}{3(1-\nu^2)\rho_s}}, \quad \beta_2 = 3.1962. \tag{47}$$

On the left-hand side of the plot, the eigenfrequencies converge to those of a clamped flat circular plate. On the right-hand side, the asymptotic value is $f_{\mathrm{INF}}/f_{P1} = 0.6470H/h$.

H. Eigenvalues with finite load at the perimeter

With a low stiffness boundary condition, β_1 and f_1 have values fairly close to β_0 and f_0, respectively, but are not

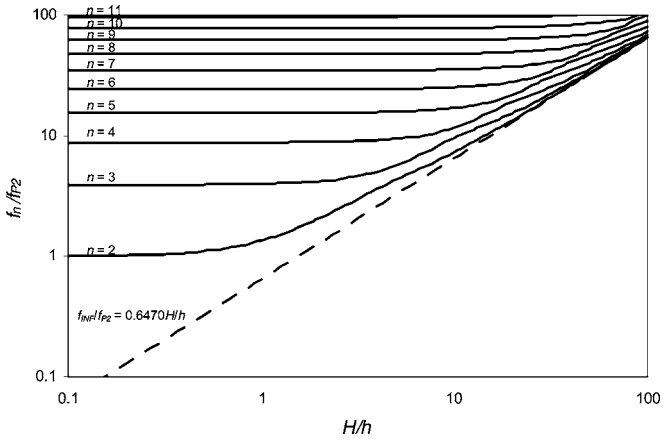

FIG. 3. Eigenfrequencies of a shallow spherical shell with infinite load at the perimeter.

coincident due to interaction between the modes. As the stiffness is increased, β_1 and f_1 approach asymptotic values representing blocked axial movement no matter how large β_0 and f_0 are.

The perimeter damping changes the angle of all the eigenvalues such that the angle of the complex eigenvalues is no longer 45° and the imaginary parts of the remainder are no longer zero.

I. Eigenfunctions

Substituting Eqs. (23), (25), and (28) in Eq. (18) yields the following eigenfunctions:

$$\eta_n(w) = J_0(\beta_n w/a) - B_n I_0(\beta_n w/a) + C_n, \tag{48}$$

which are the solutions to the following wave equation:

$$(\nabla^4 - k_S^4)(\eta_n(w) - C_n) = 0, \tag{49}$$

where

$$B_n = -\frac{\tilde{C}_3(\beta_n)}{\tilde{C}_1(\beta_n)} = -\frac{J_1(\beta_n)}{I_1(\beta_n)} \tag{50}$$

and

$$C_n = \frac{\tilde{C}_{5n}}{\tilde{C}_{1n}} = -\frac{2\xi^4(W(\beta_n) - 2(1+\nu)J_1(\beta_n)I_1(\beta_n)/\beta_n)}{(1-\nu)I_1(\beta_n)(\beta_n^4 + \xi^4)}. \tag{51}$$

III. GREEN'S FUNCTION FOR A SHALLOW SPHERICAL SHELL WITH AXIALLY SYMMETRIC EXCITATION

The Green's function for the shell that represents the particular displacement response to an axially symmetric harmonic delta excitation of unit strength may be expressed as an infinite series of modes as follows:

$$G(w|w_0) = \sum_{n=1}^{\infty} A_n \eta_n(w) \tag{52}$$

and similarly

$$C = \sum_{n=1}^{\infty} A_n C_n. \tag{53}$$

The unknown variable A_n may be solved for by substituting this Green's function in the following wave equation for a "point source" excitation at w_0, ϕ_0:

$$(\nabla^4 - k_S^4)G(w|w_0) = \frac{hY}{RD}C + \frac{1}{w}\delta(w - w_0)\delta(\phi - \phi_0). \tag{54}$$

Substituting $k_S = \beta_n/a$ in Eq. (12) yields the following identity for the Laplace operator:

$$\nabla^4 \eta_n(w) = \frac{\beta_n^4}{a^4}\eta_n + \frac{hY}{RD}C_n. \tag{55}$$

Hence

$$\nabla^4 G(w|w_0) = \sum_{n=1}^{\infty} A_n \left(\frac{\beta_n^4}{a^4}\eta_n(w) + \frac{hY}{RD}C_n \right). \tag{56}$$

Substituting Eqs. (52), (53), and (56) in the wave Eq. (54) yields

$$\sum_{n=1}^{\infty} A_n \left(\frac{\beta_n^4}{a^4} - k_S^4 \right) \eta_n(w) = \frac{1}{w}\delta(w - w_0)\delta(\phi - \phi_0), \tag{57}$$

which is then multiplied through by the eigenfunction:

$$\eta_m^*(w) = J_0(\beta_m^* w/a) - B_m^* I_0(\beta_m^* w/a) + C_m^*, \tag{58}$$

where an asterisk denotes the complex conjugate, and integrated over the surface of the shell. Due to the *orthogonality* of these functions, all terms having $m \neq n$ simply disappear. Therefore letting $m = n$ leads to

$$\frac{a^2}{2}A_n \left(\frac{\beta_n^4}{a^4} - k_S^4 \right) \int_0^{2\pi} d\phi \Delta_n = \int_0^{2\pi} \delta(\phi - \phi_0) d\phi \int_0^a \delta(w - w_0)\eta_n^*(w) dw, \tag{59}$$

where

$$\Delta_n = \frac{2}{a^2}\int_0^a \eta_n^*(w)\eta_n(w) w dw, \tag{60}$$

which is solved[18] to give

$$\begin{aligned}\Delta_n = {} & C_n C_n^* + 2\frac{\beta_n J_0(\beta_n^*)J_1(\beta_n) - \beta_n^* J_0(\beta_n)J_1(\beta_n^*)}{\beta_n^2 - \beta_n^{*2}} \\ & - 2B_n \frac{\beta_n J_0(\beta_n^*)I_1(\beta_n) + \beta_n^* I_0(\beta_n)J_1(\beta_n^*)}{\beta_n^2 + \beta_n^{*2}} \\ & - 2B_n^* \frac{\beta_n I_0(\beta_n^*)J_1(\beta_n) + \beta_n^* J_0(\beta_n)I_1(\beta_n^*)}{\beta_n^2 + \beta_n^{*2}} \\ & + 2B_n B_n^* \frac{\beta_n I_0(\beta_n^*)I_1(\beta_n) - \beta_n^* I_0(\beta_n)I_1(\beta_n^*)}{\beta_n^2 - \beta_n^{*2}} \\ & + 2C_n \frac{J_1(\beta_n^*) - B_n^* I_1(\beta_n^*)}{\beta_n^*} + 2C_n^* \frac{J_1(\beta_n) - B_n I_1(\beta_n)}{\beta_n}.\end{aligned} \tag{61}$$

If there were no damping in the system, setting $R_S = 0$ would

lead to $\beta_n^2=\beta_n^{*2}$ which would make this solution indeterminate. Hence it would be necessary to reevaluate Eq. (60) without damping in order to obtain the solution in a different form, which is not given here, since it is assumed that R_S is always nonzero. Using the property of the Dirac delta function gives the solution for A_n as follows:

$$A_n = \frac{a^2}{\pi}\frac{\eta_n^*(w_0)}{\Delta_n(\beta_n^4 - k_s^4 a^4)}. \tag{62}$$

Hence

$$G(w|w_0) = \frac{a^2}{\pi}\sum_{n=1}^{\infty}\frac{\eta_n(w)\,\eta_n^*(w_0)}{\Delta_n(\beta_n^4 - k_S^4 a^4)}. \tag{63}$$

IV. SOLUTION OF THE SHELL WAVE EQUATION WITH FLUID LOADING

The steady state wave equation for the shell can now be written adding external forces and internal resistance to the inherent shell forces given in Eq. (12),

$$(\nabla^4 - k_S'^4)\,\tilde{\eta}(w) = \frac{hY}{RD}\tilde{\psi} + \frac{\zeta}{D}\left(\frac{\delta(w-a)}{2\pi a}\tilde{F}_C - \tilde{p}_+(w) + \tilde{p}_-(w)\right), \tag{64}$$

where $\tilde{p}_+(w)$ and $\tilde{p}_-(w)=-\tilde{p}_+(w)$ are the front and rear pressure distributions, respectively, due to the surrounding acoustic medium. The modified shell wave number k_S' is related to the unmodified wave number by

$$k_S'^4 = k_S^4 - i\omega\frac{\zeta}{D}z_s, \tag{65}$$

where z_s is an arbitrary specific acoustic impedance, which, as already mentioned in Sec. I, can be used to model a mesh, sound outlet holes/mesh or a lumped cavity impedance. Combining the front and rear pressure terms, the solution for the shell deflection can be written as

$$\tilde{\eta}(w) = \frac{\zeta}{D}\int_0^{2\pi}\int_0^a\left(\frac{\delta(w_0-a)}{2\pi a}\tilde{F}_C - 2\tilde{p}_+(w_0)\right) \times G(w|w_0)w_0\,dw_0\,d\phi_0, \quad 0 \le w \le a, \tag{66}$$

where ζ is a mass loading factor given by

$$\zeta = \frac{M_S}{M_S + M_C}. \tag{67}$$

Using the modified wave number k_S', the Green's function of Eq. (63) can be written as follows:

$$G(w|w_0) = \frac{a^2}{\pi}\sum_{n=1}^{\infty}\frac{\eta_n(w)\,\eta_n^*(w_0)}{\Delta_n(\beta_n^4 - k_S'^4 a^4)}. \tag{68}$$

V. SOLUTION OF THE FREE SPACE WAVE EQUATION

As already discussed in Sec. I the shallow shell is treated here as a planar source. The monopole source elements and their images together form the shell source. Since they are coincident in the plane of the infinite baffle, they combine to form elements of double strength. Hence the shell can be modeled as a "breathing" shell in free space. Due to the symmetry of the pressure fields on either side of the plane of symmetry, there is the following Neumann boundary condition on the surface of the infinite baffle:

$$\frac{\partial}{\partial z}\tilde{p}(w,z)\big|_{z=0\pm} = -ik\rho c\tilde{u}(w) = 0, \quad a < w \le \infty. \tag{69}$$

Also, on the front and rear surfaces of the shell, there is the coupling condition

$$\frac{\partial}{\partial z}\tilde{p}(w,z)\big|_{z=0\pm}\begin{cases} = -ik\rho c\tilde{u}(w) \\ = k^2\rho c^2\tilde{\eta}(w), \quad 0 \le w \le a \end{cases} \tag{70}$$

where $\tilde{u}(w)$ is the normal particle velocity in the z direction at the surfaces and k is the wave number given by

$$k = \frac{\omega}{c} = \frac{2\pi}{\lambda}, \tag{71}$$

where ω is the angular frequency of excitation, ρ is the density of air or any other surrounding medium, c is the speed of sound in that medium, and λ is the wavelength. Values for ρ and c of 1.18 kg/m^3 and 345 m/s, respectively, are assumed. In the actual physical system (as opposed to the "breathing shell" model) the front and rear pressure distributions are related by

$$\tilde{p}(w,z) = -\tilde{p}(w,-z). \tag{72}$$

On the surface of the shell and surround, let the velocity distribution $\tilde{u}_0(w_0)$ be defined as

$$\tilde{u}_0(w_0) = \frac{\tilde{F}_C}{2\rho c S}\sum_{m=1}^{\infty}\tau_m\eta_m(w_0) = \frac{\tilde{F}_C}{2\rho c S}\sum_{m=1}^{\infty}\tau_m\left\{J_0\left(\beta_m\frac{w_0}{a}\right) - B_m I_0\left(\beta_m\frac{w_0}{a}\right) + C_m\right\}, \quad 0 \le w_0 \le a, \tag{73}$$

where S is the area defined by $S=\pi a^2$ and τ_m are the as yet unknown dimensionless eigenfunction-expansion coefficients. Using the King integral[19] and taking into account the double layer source, the pressure distribution is defined by

$$\tilde{p}(w,z) = 2\int_0^{2\pi}\int_0^a g(w,z|w_0,z_0) \times \frac{\partial}{\partial z_0}\tilde{p}(w_0,z_0)\big|_{z_0=0+}w_0\,dw_0\,d\phi_0, \tag{74}$$

where the Green's function[19] is defined in axisymmetric cylindrical coordinates by

$$g(w,z|w_0,z_0) = \frac{i}{4\pi}\int_0^{\infty}J_0(\mu w)J_0(\mu w_0)\frac{\mu}{\sigma}e^{-i\sigma|z-z_0|}d\mu \tag{75}$$

where

$$\sigma = \sqrt{k^2 - \mu^2}. \tag{76}$$

Inserting this Green's function, together with the boundary condition of Eq. (70), into the boundary integral Eq. (74) and integrating over the surface of the shell yields

$$\tilde{p}(w,z) = ka\frac{\tilde{F}_C}{2S}\int_0^\infty J_0(\mu w)\frac{a\mu}{\sigma}e^{-i\sigma z}\sum_{m=0}^{\infty}\tau_m \Xi_m(a\mu)d\mu, \tag{77}$$

where the following identity[18] has been used as follows:

$$\int_0^a J_0(\mu w_0)\,\eta_m(w_0)w_0 dw_0 = a^2\Xi_m(a\mu) \tag{78}$$

and the function Ξ_m is defined as

$$\Xi_m(a\mu) = \frac{\beta_m J_0(a\mu)J_1(\beta_m) - a\mu J_0(\beta_m)J_1(a\mu)}{\beta_m^2 - a^2\mu^2} - B_m\frac{\beta_m J_0(a\mu)I_1(\beta_m) + a\mu I_0(\beta_m)J_1(a\mu)}{\beta_m^2 + a^2\mu^2} + C_m\frac{J_1(a\mu)}{a\mu}. \tag{79}$$

Setting $z=0$, provides surface pressure as follows:

$$\tilde{p}_+(w_0) = ka\frac{\tilde{F}_C}{2S}\sum_{m=0}^{\infty}\tau_m\int_0^\infty \Xi_m(a\mu)J_0(w_0\mu)\frac{a\mu}{\sigma}d\mu. \tag{80}$$

VI. FORMULATION OF THE COUPLED PROBLEM

Substituting Eq. (80) in Eq. (66) and equating the deflection with that given by Eq. (73) [where $\tilde{\eta}(w) = -i\tilde{u}_0(w)/kc$] leads to the following coupled equation (after integrating over ϕ_0):

$$\eta_n^*(a) = -i\tau_n\frac{\Delta_{0n}(\beta_n^4 - k_S'^4a^4)D}{2ka^4\rho c^2\zeta} + 2ka\sum_{m=0}^{\infty}\tau_m\int_0^\infty \Xi_m(a\mu)\Xi_n^*(a\mu)\frac{a\mu}{\sigma}d\mu, \quad n = 1,2,\ldots, \tag{81}$$

which is obtained by equating the coefficients of $\eta_n(w)$ and again using the identity of Eq. (78).

VII. FINAL SET OF SIMULTANEOUS EQUATIONS FOR THE EIGENVALUE EXPANSION COEFFICIENTS

From Eq. (81) the following set of M simultaneous equations in τ_m can be written

$$\sum_{m=1}^{M} {}_m\Psi_n(k_S'a,ka)\tau_m = \Phi_n, \quad n = 1,\ldots,M, \tag{82}$$

where

$${}_m\Psi_n(k_S'a,ka) = -ika\frac{\Delta_n(\beta_n^4 - k_S'^4a^4)}{\zeta\alpha^2(ka)}\delta_{mn} + I(k,m,n), \tag{83}$$

$$\Phi_n = J_0(\beta_n^*) - B_n^*I_0(\beta_n^*) + C_n^*, \tag{84}$$

where

$$\alpha(ka) = a^2\omega\sqrt{\frac{2a\rho}{D}} = ka^2\sqrt{\frac{2a\gamma P_0}{D}}, \tag{85}$$

where the infinite series limit has been truncated to order M. The dimensionless parameter α is the fluid-loading factor, where P_0 is the static pressure defined by $P_0=\rho c^2/\gamma$, and δ_{mn} is the Kronecker delta function. The integral $I(k,m,n)$ is defined by

$$I(k,m,n) = I_F(k,m,n) + iI_I(k,m,n) \tag{86}$$

where

$$I_F(k,m,n) = 2k_a\int_0^k \Xi_m(a\mu)\Xi_n^*(a\mu)\frac{a\mu}{\sqrt{k^2-\mu^2}}d\mu \tag{87}$$

and

$$I_I(k,m,n) = -2ka\int_k^\infty \Xi_m(a\mu)\Xi_n^*(a\mu)\frac{a\mu}{\sqrt{\mu^2-k^2}}d\mu. \tag{88}$$

It can be seen that the numerator and denominator of the first term of Ξ_m, given by Eq. (79), are simultaneously zero when $\beta_m=a\mu$, so these are indeterminate points. Using Taylor's series, it can be shown that the function is actually continuous. Hence, the integrals can be solved numerically so long as these indeterminate points are avoided. Also, the weak singularity at $\mu=k$ in Eqs. (87) and (88) can be removed by means of suitable substitutions, as shown in the following sections. However, the integrands are strongly oscillating and the integral I_I has an infinite limit. Therefore, it is more efficient to solve these integrals analytically to yield fast converging expansions. Although the integrand contains a total of 25 terms, when Ξ_m and Ξ_n are multiplied out there are only 6 unique integrals, each subdivided into finite and infinite parts.

VIII. SOLUTION OF THE FINITE AND INFINITE INTEGRALS

A. Expansion of the finite integral

After substituting $\mu=k\sqrt{1-t^2}$, Eq. (87) for the finite integral becomes

$$I_F(k,m,n) = 2k^2a^2\int_0^1 \Xi_m(ka\sqrt{1-t^2})\Xi_n^*(ka\sqrt{1-t^2})dt, \tag{89}$$

where Ξ_m is given by Eq. (79). The Bessel functions in Eq. (89) are then expanded using the following Lommel expansions:[17]

$$J_0(ka\sqrt{1-t^2}) = \sum_{p=0}^{\infty}\frac{J_p(ka)}{p!}\left(\frac{ka}{2}\right)^p t^{2p}, \tag{90}$$

$$J_1(ka\sqrt{1-t^2}) = \sqrt{1-t^2}\sum_{p=0}^{\infty}\frac{J_{p+1}(ka)}{p!}\left(\frac{ka}{2}\right)^p t^{2p}. \tag{91}$$

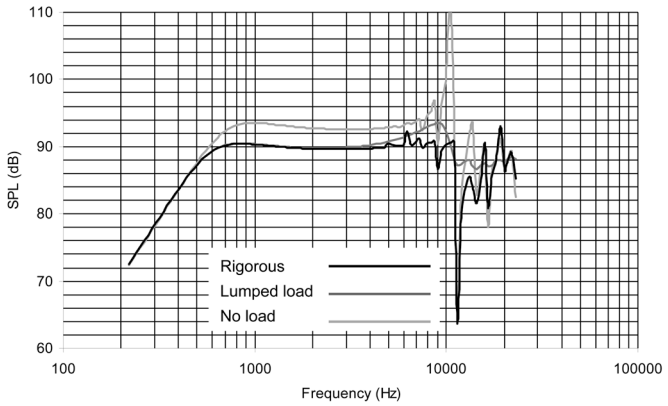

FIG. 4. On-axis far-field response with $h=10$ μm and $H=0.5$ mm ($R_M=0.06$ N s/m).

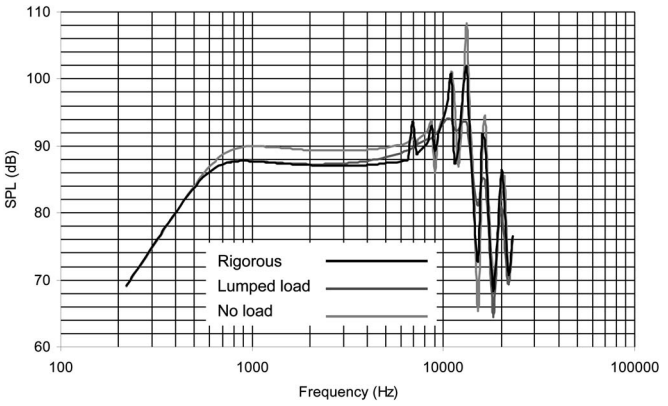

FIG. 6. On-axis far-field response with $h=20$ μm and $H=0.5$ mm ($R_M=0.13$ Ns/m).

B. Solution to the finite integral

The solution to the finite integral is given by

$$
\begin{aligned}
I_F(k,m,n) = {} & \kappa_{1a}(m,n) I_{F1}(k,\beta_m,\beta_n^*) \\
& + B_m \kappa_{1b}(m,n) I_{F1}(k,i\beta_m,\beta_n^*) \\
& + B_n^* \kappa_{1c}(m,n) I_{F1}(k,\beta_m,i\beta_n^*) \\
& + B_m B_n^* \kappa_{1d}(m,n) I_{F1}(k,i\beta_m,i\beta_n^*) \\
& + \kappa_{2a}(m,n) I_{F2}(k,\beta_m) + \kappa_{2a}(n,m) I_{F2}(k,\beta_n^*) \\
& + B_m \kappa_{2b}(m,n) I_{F2}(k,i\beta_m) \\
& + B_n^* \kappa_{2b}(n,m) I_{F2}(k,i\beta_n^*) \\
& + \kappa_{3a}(m,n) I_{F3}(k,\beta_m,\beta_n^*) \\
& + \kappa_{3a}(n,m) I_{F3}(k,\beta_n^*,\beta_m) \\
& + B_m \kappa_{3b}(m,n) I_{F3}(k,i\beta_m,\beta_n^*) \\
& + B_n^* \kappa_{3b}(n,m) I_{F3}(k,i\beta_n^*,\beta_m) \\
& + B_m B_n^* (\kappa_{3c}(m,n) I_{F3}(k,i\beta_m,i\beta_n^*) \\
& + \kappa_{3c}(n,m) I_{F3}(k,i\beta_n^*,i\beta_m)) \\
& + \kappa_{4a}(m,n) I_{F4}(k,\beta_m) + \kappa_{4a}(n,m) I_{F4}(k,\beta_n^*) \\
& - B_m \kappa_{4b}(m,n) I_{F4}(k,i\beta_m) \\
& - B_n^* \kappa_{4b}(n,m) I_{F4}(k,i\beta_n^*) \\
& + \kappa_{5a}(m,n) I_{F5}(k,\beta_m,\beta_n^*) \\
& + B_m \kappa_{5b}(m,n) I_{F5}(k,i\beta_m,\beta_n^*) \\
& + B_n^* \kappa_{5c}(m,n) I_{F5}(k,\beta_m,i\beta_n^*) \\
& + B_m B_n^* \kappa_{5d}(m,n) I_{F5}(k,i\beta_m,i\beta_n^*) \\
& + C_m C_n^* I_{F6}(k), \qquad (92)
\end{aligned}
$$

where the coefficients κ are given by Eqs. (A1)–(A22) and the solutions to the individual integral terms I_F are given by Eqs. (A23)–(A30).

C. Expansion of the infinite integral

After substituting $\mu=k\sqrt{t^2+1}$, Eq. (88) for the infinite integral becomes

$$
I_I(k,m,n) = -2k^2a^2 \int_0^\infty \Xi_m(ka\sqrt{t^2+1}) \Xi_n^*(ka\sqrt{t^2+1}) dt, \qquad (93)
$$

where Ξ_m is given by Eq. (79). The Bessel functions in Eq. (93) are then be expanded using Gegenbauer's summation theorem[15] as follows:

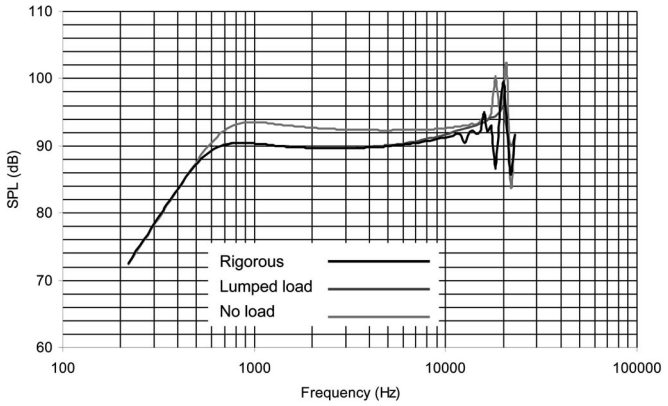

FIG. 5. On-axis far-field response with $h=10$ μm and $H=1.0$ mm ($R_M=0.06$ N s/m).

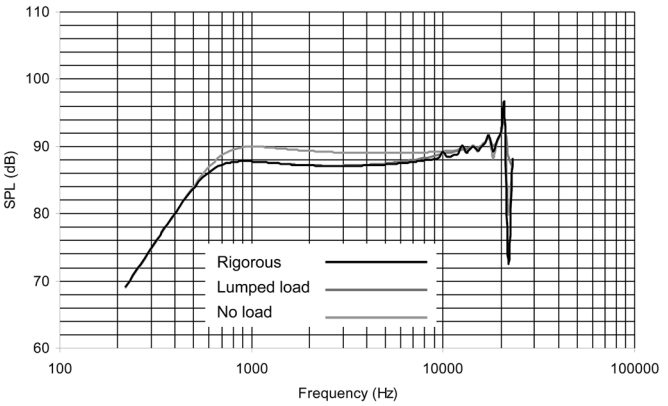

FIG. 7. (Color online) On-axis far-field response with $h=20$ μm and $H=1.0$ mm ($R_M=0.13$ Ns/m).

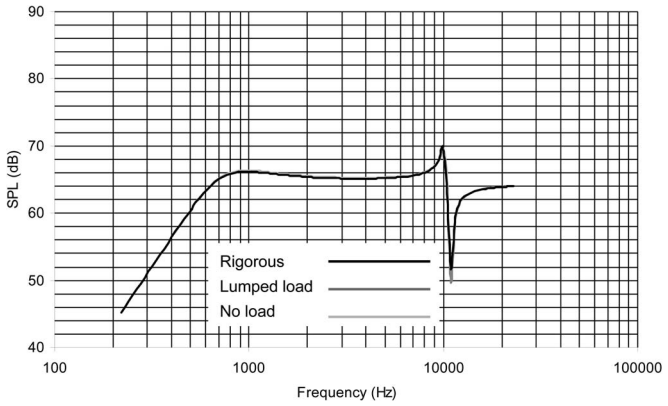

FIG. 8. On-axis far-field response with $h=475$ μm and $H=0$ mm ($R_M=3$ Ns/m).

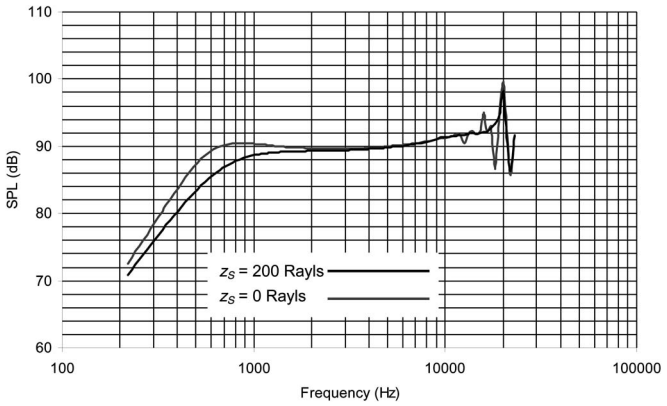

FIG. 10. On-axis far-field response with the same parameters as Fig. 5 plus an external damping resistance $z_S=200$ Ra.

$$J_0(ka\sqrt{t^2+1}) = 2\sum_{p=0}^{\infty} \frac{(-1)^p}{1+\delta_{p0}} J_{2p}(ka) J_{2p}(kat), \tag{94}$$

$$J_1(ka\sqrt{t^2+1}) = \frac{2\sqrt{t^2+1}}{kat} \sum_{p=0}^{\infty} (-1)^p (2p+1) J_{2p+1}(ka) J_{2p+1}(kat). \tag{95}$$

D. Solution to the infinite integral

The solution[18] to the infinite integral is given by

$$\begin{aligned} I_I(k,m,n) = {} & \kappa_{1a}(m,n) I_{I1}(k,\beta_m,\beta_n^*) \\ & + B_m \kappa_{1b}(m,n) I_{I1}(k,i\beta_m,\beta_n^*) \\ & + B_n^* \kappa_{1c}(m,n) I_{I1}(k,\beta_m,i\beta_n^*) \\ & + B_m B_n^* \kappa_{1d}(m,n) I_{I1}(k,i\beta_m,i\beta_n^*) \\ & + \kappa_{2a}(m,n) I_{I2}(k,\beta_m) + \kappa_{2a}(n,m) I_{I2}(k,\beta_n^*) \\ & + B_m \kappa_{2b}(m,n) I_{I2}(k,i\beta_m) \\ & + B_n^* \kappa_{2b}(n,m) I_{I2}(k,i\beta_n^*) \\ & + \kappa_{3a}(m,n) I_{I3}(k,\beta_m,\beta_n^*) \\ & + \kappa_{3a}(n,m) I_{I3}(k,\beta_n^*,\beta_m) \\ & + B_m \kappa_{3b}(m,n) I_{I3}(k,i\beta_m,\beta_n^*) \\ & + B_n^* \kappa_{3b}(n,m) I_{I3}(k,i\beta_n^*,\beta_m) \\ & + B_m B_n^* (\kappa_{3c}(m,n) I_{I3}(k,i\beta_m,i\beta_n^*) \\ & + \kappa_{3c}(n,m) I_{I3}(k,i\beta_n^*,i\beta_m)) \\ & + \kappa_{4a}(m,n) I_{I4}(k,\beta_m) + \kappa_{4a}(n,m) I_{I4}(k,\beta_n^*) \\ & - B_m \kappa_{4b}(m,n) I_{I4}(k,i\beta_m) \\ & - B_n^* \kappa_{4b}(n,m) I_{I4}(k,i\beta_n^*) \\ & + \kappa_{5a}(m,n) I_{I5}(k,\beta_m,\beta_n^*) \\ & + B_m \kappa_{5b}(m,n) I_{I5}(k,i\beta_m,\beta_n^*) \\ & + B_n^* \kappa_{5c}(m,n) I_{I5}(k,\beta_m,i\beta_n^*) \\ & + B_m B_n^* \kappa_{5d}(m,n) I_{I5}(k,i\beta_m,i\beta_n^*) + C_m C_n^* I_{I6}(k), \end{aligned} \tag{96}$$

where the coefficients κ are given by Eqs. (A1)–(A22) and the solutions to the individual integral terms I_F are given by Eqs. (A31)–(A44).

IX. FAR-FIELD PRESSURE RESPONSE: RIGOROUS CALCULATION

Starting from Eq. (73) for the surface velocity, the far-field pressure is derived using the same procedure as shown

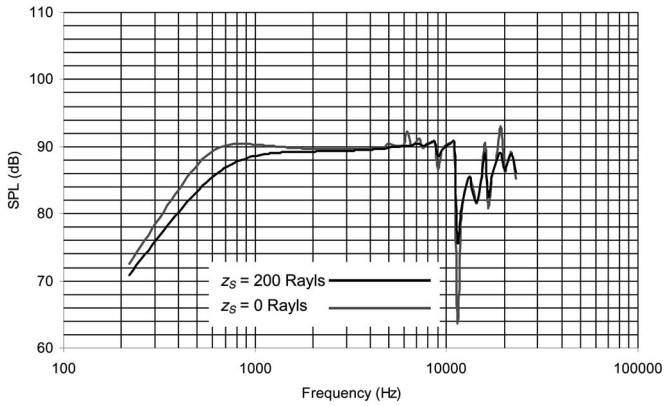

FIG. 9. On-axis far-field response with the same parameters as Fig. 4 plus an external damping resistance $z_S=200$ Ra.

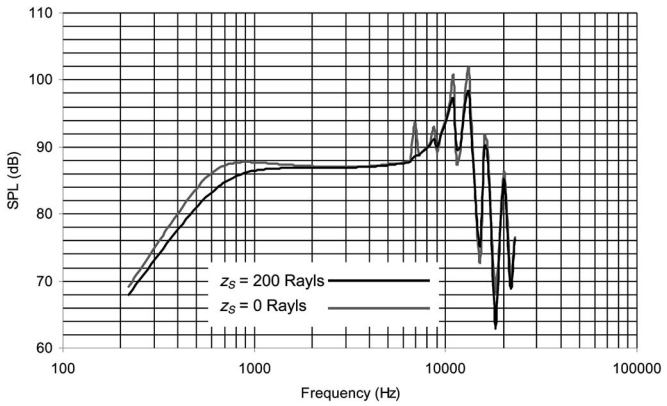

FIG. 11. On-axis far-field response with the same parameters as Fig. 6 plus an external damping resistance $z_S=200$ Ra.

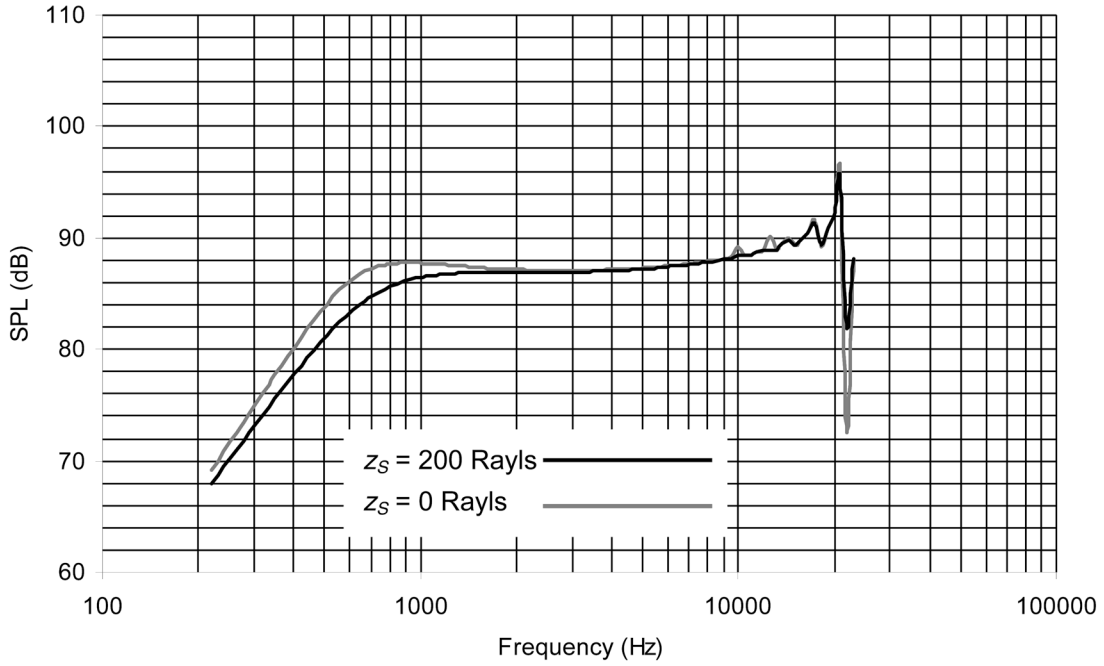

FIG. 12. (Color online) On-axis far-field response with the same parameters as Fig. 7 plus an external damping resistance z_S=200 Ra.

in Part I of Sec. II of a recent paper,[10] together with the identity of Eqs. (79) and (80) (while letting $\mu=k\sin\theta$), to give

$$\tilde{p}(r,\theta) = -i\frac{a\tilde{F}_C}{4rS}e^{-ikr}D(\theta), \tag{97}$$

where r is the distance from the center of the shell to the observation point and θ is the azimuthal angle. The directivity function $D(\theta)$ is given by

$$D(\theta) = 2ka\sum_{m=1}^{\infty}\tau_m\left(C_m\frac{J_1(ka\sin\theta)}{ka\sin\theta} - B_m \times\frac{\beta_m J_0(ka\sin\theta)I_1(\beta_m) + (ka\sin\theta)I_0(\beta_m)J_1(ka\sin\theta)}{\beta_m^2 + (ka\sin\theta)^2} + \frac{\beta_m J_0(ka\sin\theta)J_1(\beta_m) - (ka\sin\theta)J_0(\beta_m)J_1(ka\sin\theta)}{\beta_m^2 - (ka\sin\theta)^2}\right), \tag{98}$$

which, for $\theta=0$ (i.e., on-axis), simplifies to

$$D(0) = ka\sum_{m=1}^{\infty}\tau_m\left(2\frac{J_1(\beta_m)}{\beta_m} - 2B_m\frac{I_1(\beta_m)}{\beta_m} + C_m\right). \tag{99}$$

The on-axis pressure responses are shown in Figs. 4–14 using the parameters from Tables I and II where the SPL is given by

$$\mathrm{SPL} = 20\log_{10}|\tilde{p}(r,0)/20\times 10^{-6}|, \tag{100}$$

where

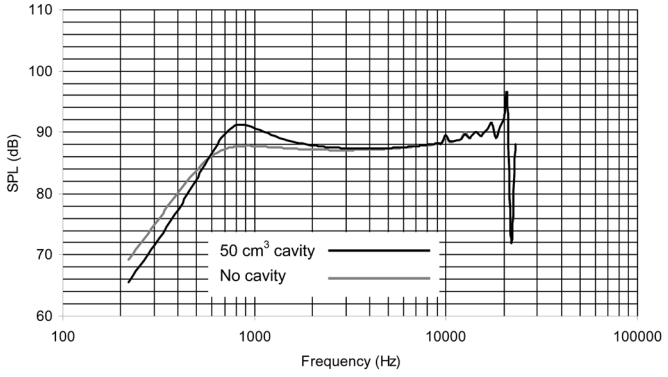

FIG. 13. (Color online) On-axis far-field response with the same parameters as Fig. 7 plus a lumped cavity with a volume of 50 cm^3.

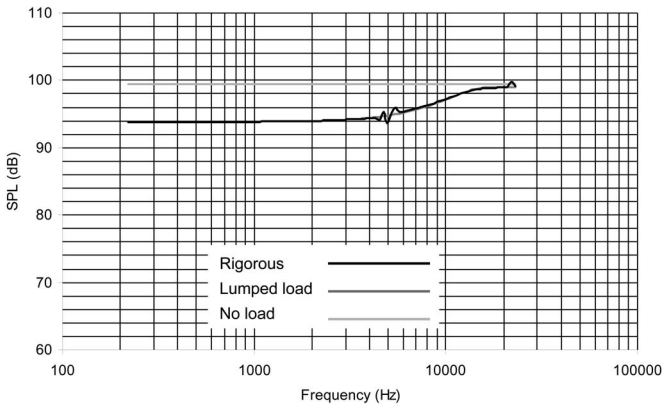

FIG. 14. On-axis far-field response with the same parameters as Fig. 4 except that the coil mass and suspension stiffness are both zero.

TABLE I. Shell parameters for the 25 mm aluminum loudspeaker.

Radius	$a=12.5$ mm
Thickness	$h=10/2/800$ μm
Apex height	$H=0/0.5/1.0$ mm
Young's modulus	$Y=69$ GN/m^2
Poisson's ratio	$\nu=0.3$
Density of shell	$\rho_S=2700$ kg/m^3
Shell mass	$M_S=\pi a^2\rho_S h=13.3/26.6/1060$ mg
Density of air	$\rho=1.18$ kg/m^3
Speed of sound in air	$c=345$ m/s
Damping/loading	$z_S=0$ kg/s unless otherwise specified
Observation distance	$r=1$ m

$$\tilde{p}(r,0)=-i\frac{ka^2\tilde{F}_C}{4rS}e^{-ikr}\sum_{m=1}^{M}\tau_m\left(2\frac{J_1(\beta_m)}{\beta_m}-2B_m\frac{I_1(\beta_m)}{\beta_m}+C_m\right). \tag{101}$$

This result can also be obtained directly by integrating the velocity $\tilde{u}_0(w_0)$ from Eq. (73) over the surface in order to derive the total volume velocity $\tilde{U}_0$ and using the standard far-field equation,[12,20]

$$\tilde{p}(r,0)=-\frac{ik\rho c\tilde{U}_0}{2\pi r}e^{-ikr}. \tag{102}$$

The calculations were performed using 80 digit precision with $M=3+2ka$ and $P=Q=2M$.

X. FAR-FIELD PRESSURE RESPONSE: WITHOUT FLUID LOADING

If the acoustic loading is ignored such that $\tilde{p}_+(w_0)=0$, Eq. (66) for the deflection can be simplified to

$$\tilde{\eta}(w)=\frac{\zeta}{D}\int_0^a\frac{\delta(w_0-a)\tilde{F}_C}{a}G(w|w_0)w_0dw_0=\frac{a^2\zeta\tilde{F}_C}{\pi D}\sum_{n=1}^{\infty}\frac{\eta_n(w)\eta_n^*(a)}{\Delta_n(\beta_n^4-k_S'^4a^4)}, \tag{103}$$

in which case

TABLE II. Coil and suspension parameters for the 25 mm aluminum loudspeaker.

Fundamental frequency	$f_0=700$ Hz
Coil electrical resistance	$R_E=7.6$ Ω
Coil wire diameter	$t=50$ μm
Coil wire density	$\rho_C=8900$ kg/m^3
Coil wire resistivity	$\sigma_C=15.9$ nΩm
Coil wire total length	$l=\pi t^2R_E/(4\sigma_C)=0.94$ m
Coil wire length per turn	$l_T=2\pi a=78.5$ mm
Coil number of turns	$n=l/l_T=12$
Coil mass	$M_C=2\pi ntp_Sh+\pi t^2l\rho_C/4=17.7/22.8/118$ mg
Magnetic flux density	$B=0.8$ T
Flux coil length product	$Bl=B\times l=0.75$ T m
Input voltage for 1 W	$\tilde{e}_{in}=\sqrt{R_E\tilde{W}}\vert_{\tilde{W}=1\text{Wrms}}=2.76$ V

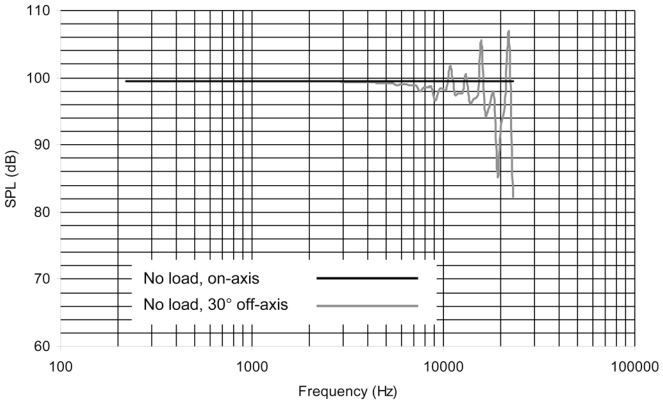

FIG. 15. 30° off-axis far-field response with the same parameters as Fig. 4 except that the coil mass and suspension stiffness are both zero.

$$\tau_m=\frac{\zeta\alpha^2(ka)(J_0(\beta_m^*)-B_m^*I_0(\beta_m^*)+C_m^*)}{ika\Delta_m(\beta_m^4-k_S'^4a^4)}, \tag{104}$$

which can be used in Eqs. (97)–(101) in order to calculate the far-field pressure response without fluid loading.

XI. DISCUSSION OF THE RESULTS

An example loudspeaker is simulated using the parameters given in Tables I and II, and the results are plotted in Figs. 4–15. Also, the eigenfrequencies in a vacuum are shown in Table III. In Figs. 4–7, results are shown for two different heights and two different thicknesses using the rigorous solution and the solution without acoustic loading. A third solution is shown which is obtained by adding the following lumped radiation impedance to the solution without loading:

$$z_S=z_{\text{Rad}}=2\rho c\left(1-\frac{J_1(2ka)}{ka}+i\frac{\mathbf{H}_1(2ka)}{ka}\right), \tag{105}$$

where z_{Rad} is the radiation impedance of a rigid disk in an infinite baffle.[12,20] It can be seen that the thin shallow shell of Fig. 4 shows significant influence from acoustic radiation load and the lumped radiation impedance is a fairly poor approximation to the rigorous solution, whereas the thicker deeper shell of Fig. 7 shows less influence and all three solutions are effectively converging. Figure 8 is for a flat plate which has been made thick

TABLE III. Eigenfrequencies for the 25 mm aluminum loudspeaker.

Frequency No.	$h=10$ μm $H=0.5$ mm	$h=10$ μm $H=1.0$ mm	$h=20$ μm $H=0.5$ mm	$h=20$ μm $H=1.0$ mm
$n=1$	699.98	699.99	700.05	700.01
$n=2$	5149.2	10313.0	5261.9	10356.0
$n=3$	5177.8	10382.0	5775.7	10629.0
$n=4$	5314.6	10573.0	6988.3	11353.0
$n=5$	5676.3	10969.0	8963.5	12756.0
$n=6$	6376.5	11659.0	11254.0	14968.0
$n=7$	7477.3	12714.0	13177.0	17981.0
$n=8$	8952.9	14178.0	16342.0	21578.0
$n=9$	10467.0	16060.0	20626.0	27911.0
$n=10$	13658.0	18324.0	25669.0	32904.0

enough to have its first "break-up" mode at the same frequency as the shell in Fig. 7. However, the penalty is drastically reduced sensitivity.

Figures 9–12 show the effect of applying acoustic resistance. Again, the thin shallow shell of Fig. 9 shows much greater influence, with a moderately damped response, than the thicker deeper shell of Fig. 12.

Figure 13 holds no surprises and simply serves to show how an approximation for a rear cavity can be included in the model using

$$z_S = z_{\mathrm{Cav}} = \frac{\rho c^2 S}{i\omega V}, \tag{106}$$

where V is the volume of the cavity and the same fully coupled acoustic loading is used as in Fig. 5. It is a lumped parameter approximation, which assumes that the cavity is anechoic at high frequencies and just provides pure compliance at low frequencies. As expected, it raises the fundamental resonant frequency and increases the associated Q_S value.

Interestingly, the on-axis response without acoustic loading or coil mass, shown in Fig. 14, is perfectly flat.[21] However, the off-axis response of Fig. 15 shows significant modal behavior, so it can be concluded that the flat on-axis response is due to the average surface velocity of the shell with a free edge (apart from a zero bending constraint) being constant at all frequencies. In Fig. 15 it can be seen that the acoustic loading disrupts this trend to a certain extent, but not as much as the coil mass in all the previous figures. Hence the effect of the mass loading from the voice coil is highly significant.

XII. CONCLUSIONS

A method for calculating the response of a loudspeaker with a diaphragm in the form of a shallow spherical shell has been derived. An example has been calculated which compares the rigorous solution with an approximation using a lumped radiation load and no load. The approximation diverges from the rigorous solution in the case of a very thin and shallow shell. Also, the effect of the mass loading from the voice coil has been explored and found to be highly significant.

ACKNOWLEDGMENT

The authors would like to express their gratitude to N. Lobo for his invaluable advice in numerical matters.

APPENDIX: SOLUTION OF THE INDIVIDUAL FINITE AND INFINITE INTEGRAL TERMS

The coefficients κ in Eqs. (92) and (96) are given by

$$\kappa_{1a}(m,n) = \beta_m \beta_n^* J_1(\beta_m) J_1(\beta_n^*), \tag{A1}$$

$$\kappa_{1b}(m,n) = \beta_m \beta_n^* I_1(\beta_m) J_1(\beta_n^*), \tag{A2}$$

$$\kappa_{1c}(m,n) = \beta_m \beta_n^* J_1(\beta_m) I_1(\beta_n^*), \tag{A3}$$

$$\kappa_{1d}(m,n) = \beta_m \beta_n^* I_1(\beta_m) I_1(\beta_n^*), \tag{A4}$$

$$\kappa_{2a}(m,n) = -C_n^* \beta_m J_1(\beta_m), \tag{A5}$$

$$\kappa_{2b}(m,n) = -C_n^* \beta_m I_1(\beta_m), \tag{A6}$$

$$\kappa_{2a}(n,m) = -C_m \beta_n^* J_1(\beta_n^*), \tag{A7}$$

$$\kappa_{2b}(n,m) = -C_m \beta_n^* I_1(\beta_n^*), \tag{A8}$$

$$\kappa_{3a}(m,n) = -\beta_m J_0(\beta_n^*) J_1(\beta_m), \tag{A9}$$

$$\kappa_{3a}(n,m) = -\beta_n^* J_0(\beta_m) J_1(\beta_n^*), \tag{A10}$$

$$\kappa_{3b}(m,n) = \beta_n^* I_0(\beta_m) J_1(\beta_n^*) - \beta_m J_0(\beta_n^*) I_1(\beta_m), \tag{A11}$$

$$\kappa_{3b}(n,m) = \beta_m I_0(\beta_n^*) J_1(\beta_m) - \beta_n^* J_0(\beta_m) I_1(\beta_n^*), \tag{A12}$$

$$\kappa_{3c}(m,n) = \beta_n^* I_0(\beta_m) I_1(\beta_n^*), \tag{A13}$$

$$\kappa_{3c}(n,m) = \beta_m I_0(\beta_n^*) I_1(\beta_m), \tag{A14}$$

$$\kappa_{4a}(m,n) = C_n^* J_0(\beta_m), \tag{A15}$$

$$\kappa_{4b}(m,n) = C_n^* I_0(\beta_m), \tag{A16}$$

$$\kappa_{4a}(n,m) = C_m J_0(\beta_n^*), \tag{A17}$$

$$\kappa_{4b}(n,m) = C_m I_0(\beta_n^*), \tag{A18}$$

$$\kappa_{5a}(m,n) = J_0(\beta_m) J_0(\beta_n^*), \tag{A19}$$

$$\kappa_{5b}(m,n) = -I_0(\beta_m) J_0(\beta_n^*), \tag{A20}$$

$$\kappa_{5c}(m,n) = -J_0(\beta_m) I_0(\beta_n^*), \tag{A21}$$

$$\kappa_{5d}(m,n) = I_0(\beta_m) I_0(\beta_n^*) \tag{A22}$$

and the solutions[18] to the individual integral terms I_F in Eq. (92) are given by

$$I_{F1}(k,\beta_m,\beta_n^*) = \int_0^1 \frac{2k^2a^2 J_0^2(ka\sqrt{1-t^2})}{(k^2a^2(1-t^2)-\beta_m^2)(k^2a^2(1-t^2)-\beta_n^{*2})} dt$$
$$= 2k^2a^2 \sum_{p=0}^{P} \sum_{q=0}^{Q} \frac{(ka/2)^{p+q} J_p(ka) J_q(ka)}{p\,!\,q\,!\,(2p+2q+1)(\beta_m^2-\beta_n^{*2})}$$
$$\times (F_{F1}(k,\beta_m,p,q) - F_{F1}(k,\beta_n^*,p,q)), \tag{A23}$$

$$I_{F2}(k,\beta_m) = \int_0^1 \frac{2ka J_0(ka\sqrt{1-t^2}) J_1(ka\sqrt{1-t^2})}{\sqrt{1-t^2}(k^2a^2(1-t^2)-\beta_m^2)} dt$$
$$= 2ka \sum_{p=0}^{P} \sum_{q=0}^{Q} \frac{(ka/2)^{p+q} J_p(ka) J_{q+1}(ka)}{p\,!\,q\,!\,(2p+2q+1)}$$
$$\times F_{F1}(k,\beta_m,p,q), \tag{A24}$$

$$I_{F3}(k,\beta_m,\beta_n^*) = \int_0^1 \frac{2k^3a^3\sqrt{1-t^2}J_0(ka\sqrt{1-t^2})J_1(ka\sqrt{1-t^2})}{(k^2a^2(1-t^2)-\beta_m^2)(k^2a^2(1-t^2)-\beta_n^{*2})}dt$$
$$= 2ka\sum_{p=0}^{P}\sum_{q=0}^{Q}\frac{(ka/2)^{p+q}J_p(ka)J_{q+1}(ka)}{p\,!\,q\,!\,(2p+2q+1)(\beta_m^2-\beta_n^{*2})}$$
$$\times(\beta_m^2F_{F1}(k,\beta_m,p,q)-\beta_n^{*2}F_{F1}(k,\beta_n^*,p,q)), \tag{A25}$$

$$I_{F4}(k,\beta_m) = \int_0^1 \frac{2k^2a^2J_1^2(ka\sqrt{1-t^2})}{k^2a^2(1-t^2)-\beta_m^2}dt$$
$$= 2k^2a^2\sum_{p=0}^{P}\sum_{q=0}^{Q}\frac{(ka/2)^{p+q}J_{p+1}(ka)J_{q+1}(ka)}{p\,!\,q!}$$
$$\times\left(\frac{F_{F1}(k,\beta_m,p,q)}{2p+2q+1}-\frac{F_{F4}(k,\beta_m,p,q)}{2p+2q+3}\right), \tag{A26}$$

$$I_{F5}(k,\beta_m,\beta_n^*) = \int_0^1 \frac{2k^4a^4(1-t^2)J_1^2(ka\sqrt{1-t^2})}{(k^2a^2(1-t^2)-\beta_m^2)(k^2a^2(1-t^2)-\beta_n^{*2})}dt$$
$$= 2\sum_{p=0}^{P}\sum_{q=0}^{Q}\frac{(ka/2)^{p+q}J_{p+1}(ka)J_{q+1}(ka)}{p\,!\,q\,!\,(2p+2q+1)}$$
$$\times\left(1-\beta_m^4\frac{F_{F1}(k,\beta_m,p,q)}{\beta_n^{*2}-\beta_m^2}+\beta_n^{*4}\frac{F_{F1}(k,\beta_n^*,p,q)}{\beta_n^*-\beta_m^2}\right), \tag{A27}$$

$$I_{F6}(k) = \int_0^1 \frac{2J_1^2(ka\sqrt{1-t^2})}{1-t^2}dt$$
$$= 1-\frac{J_1(2ka)}{ka} \tag{A28}$$

in which the subfunctions F_F are defined by the following hypergeometric functions:

$$F_{F1}(k,\beta_m,p,q) = \frac{{}_2F_1\left(1,p+q+\frac{1}{2};p+q+\frac{3}{2};\frac{k^2a^2}{k^2a^2-\beta_m^2}\right)}{k^2a^2-\beta_m^2} \tag{A29}$$

$$F_{F4}(k,\beta_m,p,q) = \frac{{}_2F_1\left(1,p+q+\frac{3}{2};p+q+\frac{5}{2};\frac{k^2a^2}{k^2a^2-\beta_m^2}\right)}{k^2a^2-\beta_m^2}. \tag{A30}$$

The solutions[18] to the individual integral terms I_I in Eq. (96) are given by

$$I_{I1}(k,\beta_m,\beta_n^*) = \int_0^\infty \frac{2k^2a^2J_0^2(ka\sqrt{t^2+1})}{(k^2a^2(t^2+1)-\beta_m^2)(k^2a^2(t^2+1)-\beta_n^{*2})}dt$$
$$= 2ka\sum_{p=0}^{P}\sum_{q=0}^{Q}\frac{J_{2p}(ka)J_{2q}(ka)}{(1+\delta_{p0})(1+\delta_{q0})(\beta_n^{*2}-\beta_m^2)}$$
$$\times(F_{I1a}(k,\beta_m,p,q)-F_{I1a}(k,\beta_n^*,p,q)-F_{I1b}(k,\beta_m,p,q)+F_{I1b}(k,\beta_n^*,p,q)), \tag{A31}$$

$$I_{I2}(k,\beta_m) = \int_0^\infty \frac{2kaJ_0(ka\sqrt{t^2+1})J_1(ka\sqrt{t^2+1})}{\sqrt{t^2+1}(k^2a^2(t^2+1)-\beta_m^2)}dt$$
$$= 2\sum_{p=0}^{P}\sum_{q=0}^{Q}\frac{(2q+1)J_{2p}(ka)J_{2q+1}(ka)}{(1+\delta_{p0})}(F_{I2a}(k,\beta_m,p,q)+F_{I2b}(k,\beta_m,p,q)), \tag{A32}$$

$$I_{I3}(k,\beta_m,\beta_n^*)$$
$$= \int_0^\infty \frac{2k^3a^3\sqrt{t^2+1}J_0(ka\sqrt{t^2+1})J_1(ka\sqrt{t^2+1})}{(k^2a^2(t^2+1)-\beta_m^2)(k^2a^2(t^2+1)-\beta_n^{*2})}dt$$
$$= 2\sum_{p=0}^{P}\sum_{q=0}^{Q}\frac{(2q+1)J_{2p}(ka)J_{2q+1}(ka)}{(1+\delta_{p0})(\beta_m^2-\beta_n^{*2})}\{F_{I3}(k,\beta_n^*,p,q)$$
$$-F_{I3}(k,\beta_m,p,q)+k^2a^2(F_{I2a}(k,\beta_m,p,q)$$
$$-F_{I2a}(k,\beta_n^*,p,q))+\beta_m^2F_{I2b}(k,\beta_m,p,q)$$
$$-\beta_n^{*2}F_{I2b}(k,\beta_n^*,p,q)\}, \tag{A33}$$

$$I_{I4}(k,\beta_m) = \int_0^\infty \frac{2k^2a^2J_1^2(ka\sqrt{t^2+1})}{k^2a^2(t^2+1)-\beta_m^2}dt$$
$$= 2\sum_{p=0}^{P}\sum_{q=0}^{Q}\frac{(2p+1)(2q+1)J_{2p+1}(ka)J_{2q+1}(ka)}{ka}$$
$$\times(k^2a^2F_{I4a}(k,\beta_m,p,q)-F_{I4b}(k,\beta_m,p,q)+\beta_m^2F_{I4c}(k,\beta_m,p,q)), \tag{A34}$$

$$I_{I5}(k,\beta_m,\beta_n^*) = \int_0^\infty \frac{2k^4a^4(t^2+1)J_1^2(ka\sqrt{t^2+1})}{(k^2a^2(t^2+1)-\beta_m^2)(k^2a^2(t^2+1)-\beta_n^{*2})}dt$$
$$= 2\sum_{p=0}^{P}\sum_{q=0}^{Q}\frac{(2p+1)(2q+1)J_{2p+1}(ka)J_{2q+1}(ka)}{ka(\beta_m^2-\beta_n^{*2})}$$
$$\times\{k^4a^4(F_{I4a}(k,\beta_m,p,q)-F_{I4a}(k,\beta_n,p,q))$$
$$-(k^2a^2+\beta_m^2)F_{I4b}(k,\beta_m,p,q)+(k^2a^2$$
$$+\beta_n^{*2})F_{I4b}(k,\beta_n^*,p,q)+\beta_m^4F_{I4c}(k,\beta_m,p,q)$$
$$-\beta_n^{*4}F_{I4c}(k,\beta_n^*,p,q)\}, \tag{A35}$$

$$I_{I6}(k) = \int_0^\infty \frac{2J_1^2(ka\sqrt{t^2+1})}{t^2+1}dt = \frac{\mathbf{H}_1(2ka)}{ka}, \tag{A36}$$

in which $\mathbf{H}$ is the Struve function and the subfunctions F_I are defined by the following hypergeometric and hyperbolic Bessel functions:

$$F_{I1a}(k,\beta_m,p,q) = \frac{{}_3F_4\left(1,1,\frac{3}{2};\frac{3}{2}-p-q,\frac{3}{2}+p-q,\frac{3}{2}-p+q,\frac{3}{2}+p+q;k^2a^2-\beta_m^2\right)}{\pi(p-q-1/2)_2(p+q-1/2)_2}, \tag{A37}$$

$$F_{I1b}(k,\beta_m,p,q) = \frac{2\pi I_{2p}(\sqrt{k^2a^2-\beta_m^2})I_{2q}(\sqrt{k^2a^2-\beta_m^2})}{\sqrt{k^2a^2-\beta_m^2}}, \tag{A38}$$

$$F_{I2a}(k,\beta_m,p,q) = \frac{{}_3F_4\left(1,\frac{3}{2},2;\frac{3}{2}-p-q,\frac{3}{2}+p-q,\frac{5}{2}-p+q,\frac{5}{2}+p+q;k^2a^2-\beta_m^2\right)}{\pi(p-q-3/2)_3(p+q-1/2)_3}, \tag{A39}$$

$$F_{I2b}(k,\beta_m,p,q) = \frac{2\pi I_{2p}(\sqrt{k^2a^2-\beta_m^2})I_{2q+1}(\sqrt{k^2a^2-\beta_m^2})}{k^2a^2-\beta_m^2}, \tag{A40}$$

$$F_{I3}(k,\beta_m,p,q) = 2\frac{{}_3F_4\left(\frac{1}{2},1,1;\frac{1}{2}-p-q,\frac{1}{2}+p-q,\frac{3}{2}-p+q,\frac{3}{2}+p+q;k^2a^2-\beta_m^2\right)}{\pi(p-q-1/2)(p+q+1/2)}, \tag{A41}$$

$$F_{I4a}(k,\beta_m,p,q) = 3\frac{{}_3F_4\left(1,2,\frac{5}{2};\frac{3}{2}-p-q,\frac{5}{2}+p-q,\frac{5}{2}-p+q,\frac{7}{2}+p+q;k^2a^2-\beta_m^2\right)}{2\pi(p-q-3/2)_4(p+q-1/2)_4}, \tag{A42}$$

$$F_{I4b}(k,\beta_m,p,q) = \frac{{}_3F_4\left(1,1,\frac{3}{2};\frac{1}{2}-p-q,\frac{3}{2}+p-q,\frac{3}{2}-p+q,\frac{5}{2}+p+q;k^2a^2-\beta_m^2\right)}{\pi(p-q-1/2)_2(p+q+1/2)_2}, \tag{A43}$$

$$F_{I4c}(k,\beta_m,p,q) = \frac{2\pi I_{2p+1}(\sqrt{k^2a^2-\beta_m^2})I_{2q+1}(\sqrt{k^2a^2-\beta_m^2})}{(k^2a^2-\beta_m^2)^{3/2}}. \tag{A44}$$

[1] E. Reissner, On axi-symmetrical vibrations of shallow spherical shells, Q. Appl. Math. **13**, 279–290 (1955).
[2] M. W. Johnson and E. Reissner, On transverse vibrations of shallow spherical shells, Q. Appl. Math. **15**, 367–380 (1956).
[3] A. W. Leissa, *Vibrations of Shells* (Acoustical Society of America, New York, 1993).
[4] R. Jones and J. Mazumdar, Transverse vibrations of shallow shells by the method of constant-deflection contours, J. Acoust. Soc. Am. **56**, 1487–1492 (1974).
[5] O. Thomas, C. Touzé, and A. Chaigne, Non-linear vibrations of free-edge thin spherical shells: Modal interaction rules and 1:1:2 internal resonance, Int. J. Solids Struct. **42**, 3339–3373 (2005).
[6] J. C. Snowdon, Forced vibration of internally damped circular plates with supported and free boundaries, J. Acoust. Soc. Am. **47**, 882–891 (1970).
[7] H. Suzuki and J. Tichy, Sound radiation from convex and concave domes in an infinite baffle, J. Acoust. Soc. Am. **69**, 41–49 (1981).
[8] H. Suzuki and J. Tichy, Sound radiation from an elastically supported circular plate, J. Acoust. Soc. Am. **65**, 106–111 (1979).
[9] T. J. Mellow and L. M. Kärkkäinen, On the sound field of a membrane in free space and an infinite baffle, J. Acoust. Soc. Am. **120**, 2460–2477 (2006).
[10] T. J. Mellow, On the sound field of a resilient disk in an infinite baffle, J. Acoust. Soc. Am. **120**, 90–101 (2006)
[11] C. J. Bouwkamp, Theoretical and numerical treatment of diffraction through a circular aperture, IEEE Trans. Antennas Propag. **AP18-2**, 152–176 (1970).
[12] T. J. Mellow and L. M. Kärkkäinen, On the sound field of an oscillating disk in a finite open and closed circular baffle, J. Acoust. Soc. Am. **118**, 1311–1325 (2005).
[13] S. Timoshenko and S. Woinowsky-Kreiger, *Theory of Plates and Shells* (McGraw-Hill, New York, 1959), pp. 36–42, 79–88, 429–435, 533–559.
[14] M. H. Gradowczyk, "Some remarks on the theory of shallow spherical shells," Ing.-Arch. **32**, 297–303 (1963).
[15] I. S. Gradshteyn and I. M. Ryzhik, *Table of Integrals, Series, and Products*, 6th ed., edited by A. Jeffrey (Academic, New York, 2000), p. 934, Eqs. (8.561.1) and (8.561.2), p. 935, Eqs. (8.567.1) and (8.567.2), p. 916, Eqs. (8.471.1) and (8.471.2), p. 918, Eqs. (8.486.1) and (8.486.2), p. 930, Eq. (8.532.1), p. 980, Eqs. (8.930.1)–(8.930.7).
[16] G. B. Arfken and H. J. Weber, *Mathematical Methods for Physicists*, 6th ed. (Academic, 2005), p. 723, Eq. (11.137), p. 722, Eq. (11.136).
[17] G. N. Watson, *A Treatise on the Theory of Bessel Functions*, 2nd ed., (Cambridge University Press, London, 1944), 141 pp., Sec. 5.22, Eq. (5).
[18] S. Wolfram, *The Mathematica Book*, 5th ed. (Wolfram Media, Champaign, IL, 2003). Symbolic computation by Mathematica.
[19] P. M. Morse and K. U. Ingard, *Theoretical Acoustics* (McGraw-Hill, New York, 1968), pp. 320, 321, 365.
[20] L. L. Beranek, *Acoustics* (Acoustical Society of America. New York, 1993), p. 188, Eq. (7.7), p. 118, Eq. (5.1).
[21] N. Harris and G. Bank, "A balanced modal radiator," on the CD ROM: Audio Engineering Society Convention Papers, 119th Convention Paper 6595, New York, 7–10 October 2005, available from Audio Engineering Society Inc., 60 East 42nd Street, Rm. 2520, New York, NY 10165–2520.